Hindawi
Wireless Communications and Mobile Computing
Volume 2022, Article ID 5498172, 11 pages
https://doi.org/10.1155/2022/5498172

Research Article

Secrecy Energy Efficiency Optimization for Reconfigurable Intelligent Surface-Aided Multiuser MISO Systems

Jinhong Bian, YuanYuan Wang, and Feng Zhou

School of Information Technology, Yancheng Institute of Technology, Yancheng 224051, China

Correspondence should be addressed to Jinhong Bian; bianjh@ycit.edu.cn

Received 12 February 2022; Revised 12 September 2022; Accepted 28 September 2022; Published 7 October 2022

Academic Editor: Xingwang Li

Copyright © 2022 Jinhong Bian et al. This is an open access article distributed under the Creative Commons Attribution License, which permits unrestricted use, distribution, and reproduction in any medium, provided the original work is properly cited.

Currently, the reconfigurable intelligent surface (RIS) has been applied to improve the physical layer security in wireless networks. In this paper, we focus on the secure transmission in RIS-aided multiple-input single-output (MISO) systems. Specifically, by assuming that only imperfect channel state information (CSI) of the eavesdropper can be obtained, we investigated the robust secrecy energy efficiency (SEE) optimization via jointly designing the active beamforming (BF), artificial noise (AN) at Alice, and the passive phase shifter at the RIS. The formulated problem is hard to handle due to the complicated secrecy rate expression as well as the infinite constraints introduced by the CSI uncertainties. By utilizing the Taylor expansion, we transformed the fractional programming into a convex problem, while all the constraints are approximated via the successive convex approximation and constrained concave-convex procedure. Then, by using the extended S-Lemma, we transform the infinite constraints into linear matrix inequality, which is convex. Finally, an alternate optimization (AO) algorithm was proposed to solve the reformulated problem. Simulation results demonstrated the performance of the proposed design.

1. Introduction

Recently, the energy efficiency (EE) has been regarded as an important aspect in assessing the performance of communication systems, which is defined as the ratio of the information rate to the total power consumption [1]. Meanwhile, the reconfigurable intelligent surface (RIS) has been emerged as a promising technique to improve the performance such as coverage, throughput, spectrum efficiency (SE), and EE of future wireless networks [2, 3].

To be specific, Fang et al. [4] studied the EE optimization of RIS-enabled nonorthogonal multiple access (NOMA) networks, where a semidefinite relaxation- (SDR-) based algorithm was proposed to optimize the transmit and passive BF. Then, [5] investigated the EE-oriented resource allocation for RIS-assisted uplink systems by using a block coordinate descent- (BCD-) based method. Then, Le et al. [6, 7] studied the EE optimization in RIS-assisted cell-free multiple-input single-output (MISO) and multiple-input multiple-output (MIMO) network, respectively. Moreover, Yang et al. [8–10] investigated the EE optimization of distributed wireless network, device-to-device network, and wireless energy harvesting network, respectively. Recently, Yuo et al. [11] studied the EE and SE tradeoff in RIS-aided MIMO network, where an iterative mean-square error minimization approach was developed to optimize the phase shifter. On the other hand, in [12], Wang et al. studied the cooperative hybrid NOMA-based mobile-edge computing networks. In [13], Wang et al. studied the delay-sensitive secure NOMA transmission for Internet-of-Things (IoT) networks. Then, Wang et al. [14] investigated the outage-driven link selection for secure buffer-aided networks. Moreover, He et al. [15] investigated a NOMA-enabled framework for relay deployment and network optimization in airborne access vehicular ad hoc networks.

Besides the benefits of improving the SE or EE, the application of RIS is also appealing in secure communication application. For example, Dong and Wang [16] studied the secure MIMO transmission enhanced by a RIS, where a BCD-based method was proposed to design the precoding and phase shifter. Then, a minorization-maximization- (MM-) based method was proposed to optimize the precoding, artificial noise (AN) covariance and the phase shifter for secure MIMO network in [17]. Actually, if the phase shifts are given, the optimization problem reduces to a conventional beamforming (BF) design problem in MISO network, which has been extensively studied in the literature. Inspired by this consideration, alternating optimization (AO) algorithms are usually applied to decouple the optimization variables. Then, the BF vectors at the Tx are typically obtained by using existing BF design methods such as the weighted minimum mean square error (WMMSE) algorithm [18]. On the other hand, the optimization methods of the phase shifts in RIS-assisted network can be summarized as follows: (a) optimization techniques for continuous phase shifts: (1) relaxation and projection; (2) SDR; (3) majorization-minimization (MM) algorithm; (4) manifold approach; (5) element-wise BCD; (6) alternating direction method of multipliers (ADMM) based algorithm; (7) penalty convex-concave procedure (PCCP); (8) barrier function penalty; (9) accelerated projected gradient; (10) deep reinforcement learning. (b) Optimization techniques for discrete phase shifts: (1) rounding method; (2) binary mode selection method; (3) negative square penalty [19].

The performance index of these works were commonly measured by the criterion called secrecy rate, which is the capacity of conveying information to the legitimated users (Bobs), while keeping it confidential from the eavesdroppers (Eves) [20]. However, for network design with both security and EE requirements, it is beneficial to combine these two metrics into an individual target, which is termed as the secrecy EE (SEE) and defined as the ratio between the achieved secrecy rate to the total power consumption. Specifically, Wu et al. [21] studied the SEE maximization in RIS-assisted cognitive radio system, where a Dinkelbach and second order cone programming- (SOCP-) based method was proposed. Also, Wang et al. [22] studied the robust BF and cooperative jamming design in a RIS-assisted MISO network to maximize the SEE, where an AO algorithm was developed. Recently, Liu et al. [23] studied the SEE in RIS-aided secure simultaneous wireless information and power transfer (SWIPT) network, where an AO-based method was proposed.

The acquirement of the channel state information (CSI) is an important issue in communication network. Currently, the methods of the channel estimation for the RIS-aided network can be divided into two folds. The first one is to estimate the transmitter (Tx)-RIS channel and the RIS-user channel separately by installing some active elements at the RIS, which requires more hardware and power consumption [24]. The second method is to estimate the cascaded Tx-RIS-user channel, e.g., the product of the Tx-RIS channel and the RIS-user channel, where the main advantage is that no extra hardware and power cost are needed [25], and actually the cascaded channel is sufficient for the joint BF design [26]. However, in secure communication scenario, since the Eves are commonly passive nodes, it is very hard to obtain the perfect CSI of the Eves.

In existing works, the CSI of the Eves are commonly model as the bounded error model and the statistical error model. For the bounded CSI errors, in [27], Zhou et al. studied the worst-case robust BF design for RIS-aided MISO communication systems to maximize the worst case information rate. Then, Yu et al. [28] studied the worst-case robust secrecy design in RIS-assisted network with bounded CSI errors. Besides, for the statistical error model, in [29], Zhao et al. studied the outage-constrained robust BF for RIS-aided wireless communication. Also, in [30, 31], the authors studied the outage-constrained BF in RIS-assisted secure network. Then, in [20, 32], the authors studied both the two kinds of robust design in RIS-aided multiuser system and secure SWIPT system, respectively. Recently, in [33], Hong et al. proposed a novel On/Off scheme for the RIS to improve the robustness. However, these works mainly focused on the secrecy rate optimization; the SEE in RIS-aided multiuser downlink network has not been studied yet.

Motivated by these observations, in this paper, we investigate the robust SEE design in a downlink multiuser MISO network. The main contributions are summarized as follows:

(i) by assuming that only imperfect CSI of the Eve can be obtained, we aim to maximize the worst case SEE by jointly designing the active BF and AN at Alice, and the passive phase shifter at the RIS. The formulated problem is hard to handle due to the complicated secrecy rate expression as well as the infinite constraints introduced by the CSI uncertainty

(ii) differently with the commonly used Dinkelbach algorithm, which turn the fractional objective into a subtractive form, we equivalently transform it into a more tractable reformulation with linear objective via successive convex approximation (SCA) and constrained concave-convex procedure (CCCP). Then, by using the extended S-Lemma, we transform the infinite constraints into linear matrix inequality, which is convex

(iii) finally, an AO algorithm was proposed to solve the reformulated problem. Simulation results demonstrated the performance of the proposed design and provide some meaningful insights. (1) RIS plays more important role than AN in enhancing the SEE; (2) less number of quantization bits can lead to higher SEE; (3) the acquirement of the CSI is important in secrecy transmission design

The rest of this paper is organized as follows. A system model and problem formulation is given in Section 2. Section 3 investigates the joint BF, AN, and phase shifter design, wherein a SCA and CCCP based iterative approach is proposed. Simulation results are illustrated in Section 4. Section 5 concludes this paper.

Notations: Throughout the paper, we use the upper case boldface letters for matrices and lower case boldface letters for vectors. The conjugate, transpose, conjugate transpose, and trace of matrix A are denoted as A^*, A^T, A^H, and Tr(A), respectively. $a = \mathrm{vec}(A)$ means to stack the columns of A into a. $A \pm 0$ means that A is positive semidefinite. Besides, $\mathrm{Diag}(x_1, \cdots, x_N)$ represents a diagonal matrix with $x_1, \cdots, x_N$ on the main diagonal. $\|\cdot\|_2$ and $\|\cdot\|_F$ denote the Euclidean norm and Frobenius norm, respectively. I indicates an identity matrix. Moreover, $\Re\{a\}$, $|a|$, and $\angle a$ denote the real part, the modulus, and the angle of a complex number a, respectively. The distribution of a circularly symmetric complex Gaussian (CSCG) random vector with mean x and covariance Σ is denoted by $CN(x, \Sigma)$. In addition, $\circ$ means the Hadamard production; $\otimes$ denotes the Kronecker product, and $\mathbb{E}\{\cdot\}$ means the mathematical expectation, respectively.

2. System Model and Problem Formulation

2.1. System Model. We consider a downlink multiuser MISO system as shown in Figure 1, which consists of one transmitter (Alice), one RIS, K Bobs, and K Eves. The Alice and the RIS are equipped with N antennas and M reflecting elements, respectively, while all Bobs and Eves are single antenna nodes. We denote $F \in \mathbb{C}^{N\times M}$, $g_k \in \mathbb{C}^{N\times 1}$, $h_k \in \mathbb{C}^{M\times 1}$, $g_{e,k} \in \mathbb{C}^{N\times 1}$, and $h_{e,k} \in \mathbb{C}^{M\times 1}$, as the channels between Alice and RIS, between Alice and the k-th Bob, between RIS and the k-th Bob, between Alice and the k-th Eve, and between RIS and the k-th Eve, respectively. In addition, we assume that a RIS controller is utilized to exchange the CSI between Alice and the RIS. Besides, the controller adjusts the phase shift and amplitude of each passive element at the RIS to achieve passive BF so that the signal power is improved at the Bobs or reduced at the Eves.

Alice sends K independent data streams for each Bob in the same frequency band, under the thread of the Eves. Let us denote s_k as the confidential message intended to the k-th Bob, with $\mathbb{E}\{|s_k|^2\} = 1$. Since AN is injected to degrade the Eve's channel, the transmitted signal is given as $x = \sum_{k=1}^{K} w_k s_k + v$, where $w_k \in \mathbb{C}^{N\times 1}$ denotes the BF vector intent to the k-th Bob, and $v \in \mathbb{C}^{N\times 1}$ denotes the AN vector.

In this work, we assume that each Eve only eavesdrop the signal send to the nearest Bob. Thus, the received signals at the k-th Bob and the k-th Eve are, respectively, given by

$$y_k = \left(g_k^H + h_k^H \Theta^H F\right)\left(\sum_{k=1}^{K} w_k s_k + v\right) + n_k, \tag{1a}$$

$$y_{e,k} = \left(g_{e,k}^H + h_{e,k}^H \Theta^H F\right)\left(\sum_{k=1}^{K} w_k s_k + v\right) + n_{e,k}, \tag{1b}$$

where n_k and $n_{e,k}$ are the zero-mean additive Gaussian noise at the k-th Bob and Eve, with variance σ_k^2 and $\sigma_{e,k}^2$, respectively.

Here, we assume that the Bobs have the priori knowledge about the AN vector v. Thus, Bobs can cancel the interference and the actually received signal at the k-th Bob is given by $y_k = (g_k^H + h_k^H \Theta^H F)\sum_{k=1}^{K} w_k s_k + n_k$.

Here, Θ denotes an $M \times M$ diagonal reflection coefficient matrix (also known as the passive BF matrix), which can be written as $\Theta = \mathrm{Diag}(\theta_1, \cdots, \theta_M)$, $\theta_m = e^{j\varphi_m}, \varphi_m \in [0, 2\pi), \forall m \in M\Delta = \{1, \cdots, M\}$. Let Q denote the number of quantization bits for phase-shift control per RIS element, respec-

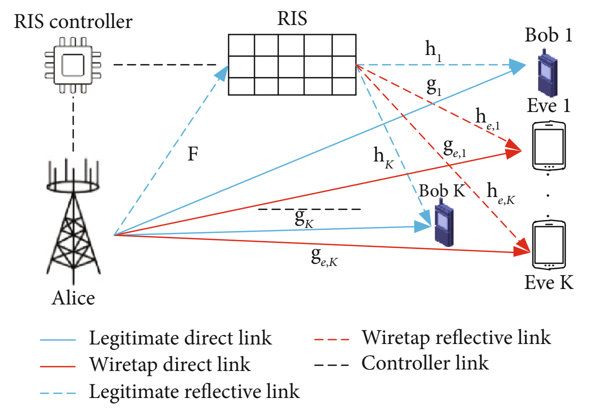

Figure 1: The system model for the RIS-assisted secure network.

tively. We thus have

$$\theta_m \in X_d \Delta = \left\{\theta_m \middle| \theta_m = e^{j\varphi_m}, \varphi_m \in S\right\}, \tag{2}$$

where $S\Delta = \{0, (2\pi/L), \cdots, (2\pi(L-1)/L)\}$ with $L = 2^Q$, i.e., the discrete phase-shift values are assumed to be equally spaced in a circle. Furthermore, by letting $Q \longrightarrow \infty$, the model in (2) becomes the case with continuous phase shifts, i.e., $\theta_m \in X_c \Delta = \{\theta_m \| \theta_m| = 1\}$. In practice, due to the hardware limitation, it is costly to achieve continuous phase shift on the reflecting elements. However, it is meaningful to investigate the continuous phase shift design, since the optimization method for the continuous phase shift is useful to the discrete phase shift design.

In fact, by denoting $\boldsymbol{\theta} = [\theta_1, \cdots, \theta_M]^T$, we have

$$\begin{aligned}\left(g_k^H + h_k^H \Theta^H F\right) w_k &= \boldsymbol{\theta}^H \underbrace{\mathrm{Diag}\left(h_k^H\right) F}_{H_k} w_k + g_k^H w_k \\ &= \underbrace{\left[\boldsymbol{\theta}^H 1\right]}_{\widehat{\boldsymbol{\theta}}^H} \underbrace{\left[H_k, g_k\right]^T}_{\bar{H}_k} w_k = \widehat{\boldsymbol{\theta}}^H \bar{H}_k w_k,\end{aligned} \tag{3}$$

and

$$\begin{aligned}\left(g_{e,k}^H + h_{e,k}^H \Theta^H F\right) w_k &= \boldsymbol{\theta}^H \underbrace{\mathrm{Diag}\left(h_{e,k}^H\right) F}_{H_{e,k}} w_k + g_{e,k}^H w_k \\ &= \widehat{\boldsymbol{\theta}}^H \underbrace{\left[H_{e,k}, g_{e,k}\right]^T}_{\bar{H}_{e,k}} w_k = \widehat{\boldsymbol{\theta}}^H \bar{H}_{e,k} w_k.\end{aligned} \tag{4}$$

Thus, the signal-to-interference-plus-noise ratio (SINR)

1.	**Initialization**: $l = 1$, set P_s, F, h_k, h_e, g_k, g_e and the initial value $\{w_k^1, v^1, \widehat{\boldsymbol{\theta}}^1\}$.
2:	**Repeat**
	(a) Obtain $\{w_k^l, v^l\}$ with fixed $\widehat{\boldsymbol{\theta}}$ by solving P5.
	(b) Obtain $\widehat{\boldsymbol{\theta}}^l$ with fixed $\{w_k, v\}$ by solving P6.
	(c) $l = l + 1$.
3:	**Until** $WSR^{l+1} - WSR^l \leq \varsigma$.
4:	**Output** $\{w_k^{\mathring{a}}, v^{\mathring{a}}, \widehat{\boldsymbol{\theta}}^{\mathring{a}}\}$.

Algorithm 1: The AO Algorithm for P1.

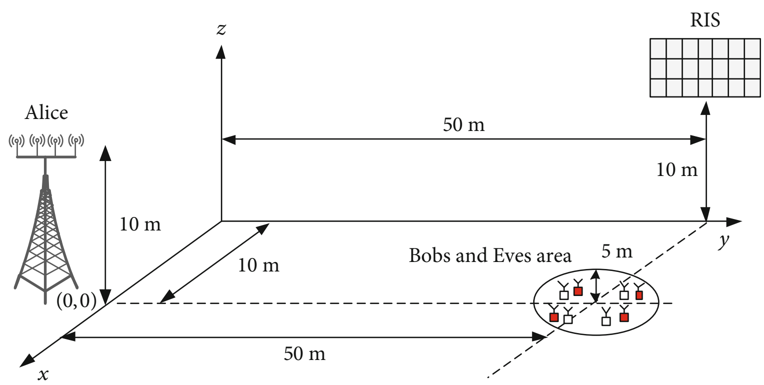

Figure 2: The deployment of the simulation scenario.

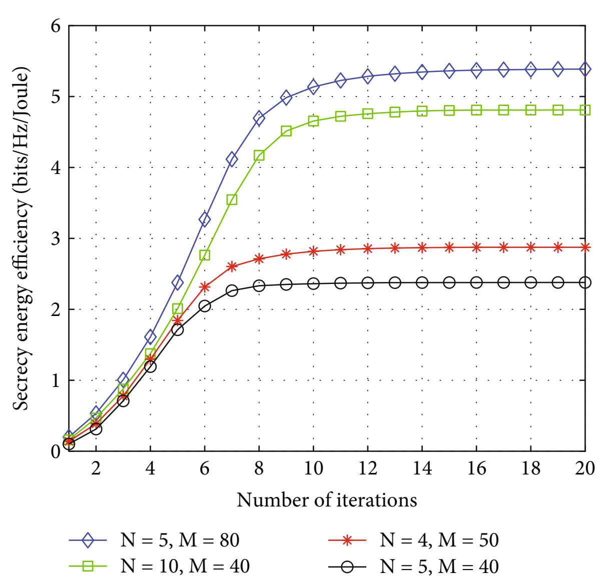

Figure 3: Convergence behaviour.

at the k-th BoB and the k-th Eve can be given as

$$\Gamma_k = \frac{\left|\widehat{\boldsymbol{\theta}}^H \bar{H}_k w_k\right|^2}{\sum_{i=1, i\neq k}^K \left|\widehat{\boldsymbol{\theta}}^H \bar{H}_k w_i\right|^2 + \sigma_k^2}, \tag{5a}$$

$$\Gamma_{e,k} = \frac{\left|\widehat{\boldsymbol{\theta}}^H \bar{H}_{e,k} w_k\right|^2}{\sum_{i=1, i\neq k}^K \left|\widehat{\boldsymbol{\theta}}^H \bar{H}_{e,k} w_i\right|^2 + \left|\widehat{\boldsymbol{\theta}}^H \bar{H}_{e,k} v\right|^2 + \sigma_e^2}, \tag{5b}$$

respectively.

Hence, the information rates at the k-th Bob and the Eve are, respectively, given by

$$C_k\left(w_k, v, \widehat{\boldsymbol{\theta}}\right) = \log_2(1 + \Gamma_k), \tag{6a}$$

$$C_{e,k}\left(w_k, v, \widehat{\boldsymbol{\theta}}\right) = \log_2(1 + \Gamma_{e,k}). \tag{6b}$$

Thus, the secrecy rate for the RIS-assisted network is given by

$$R_s\left(w_k, v, \widehat{\boldsymbol{\theta}}\right) = \min_{\forall k \in [1,\cdots,K]} \left\{C_k\left(w_k, v, \widehat{\boldsymbol{\theta}}\right) - C_{e,k}\left(w_k, v, \widehat{\boldsymbol{\theta}}\right)\right\}. \tag{7}$$

Similar to [11], the total power consumption of the network is model as

$$P\left(w_k, v, \widehat{\boldsymbol{\theta}}\right) = \frac{P_s}{\eta_s} + P_c + MP_{\mathrm{RIS}}(Q), \tag{8}$$

where $P_s = \sum_{k=1}^K \|w_k\|^2 + \|v\|^2$ denotes the transmit power; $0 \leq \eta_s \leq 1$ is the power amplifier efficiency for Alice. In addition, the constant P_c denotes the total circuit power

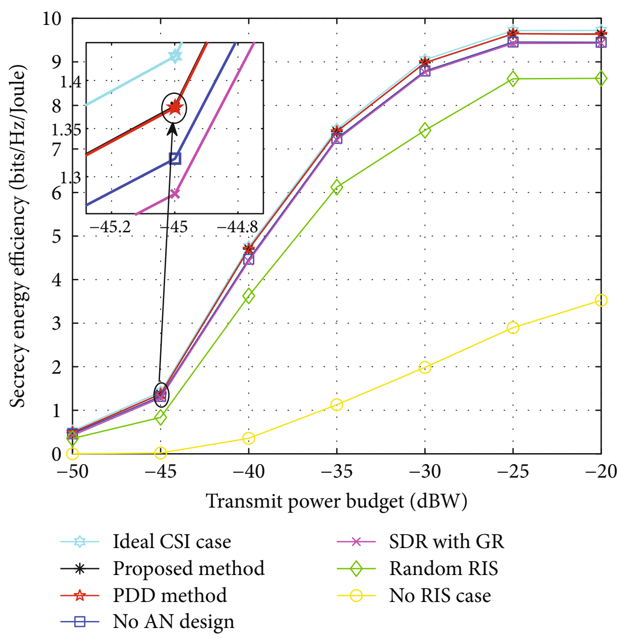

FIGURE 4: The SEE versus $P_{\max}$.

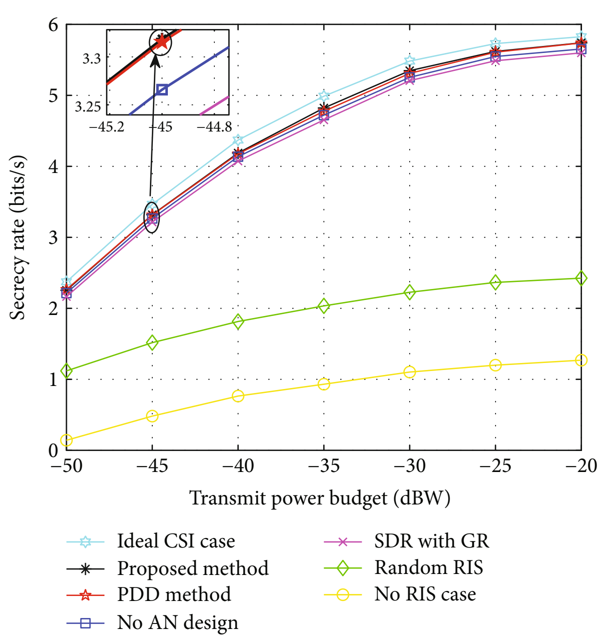

FIGURE 5: The secrecy rate versus $P_{\max}$.

consumption for Alice and the receivers. Without loss of generality, we assume $\eta_s = 1$ in the following part, [10, 21, 23]. Besides, $P_{\text{RIS}}(Q)$ denotes the per unit hardware dissipated power at the RIS with a Q-bit resolution phase shifter. From (11), we can observe that the RIS operates without consuming any transmit power, since RIS is a passive device which do not change the magnitude of the reflected signals. (According to [3], the typical power consumption values of each phase shifter are 1.5, 4.5, 6.0, and 7.8mW for 3-, 4-, 5 -, and 6-bit resolution phase shifting.) According to several related works such as [3–5], the linear power consumption model is rational when the following assumptions holds. First, the static circuit power P_c is independent of the data rate. Second, the power amplifier at Alice operates in the linear region, thus a constant power offset can approximate the hardware power consumption. Typical wireless communication transceivers satisfy these two assumptions generally.

Therefore, the SEE for the RIS-aided network is defined as

$$SEE\left(w_k, v, \widehat{\boldsymbol{\theta}}\right) = \frac{R_s\left(w_k, v, \widehat{\boldsymbol{\theta}}\right)}{P\left(w_k, v, \widehat{\boldsymbol{\theta}}\right)}. \tag{9}$$

2.2. CSI Error Models. In this work, both imperfect direct link and cascaded link are considered, i.e., we model $H_{e,k}$ and $g_{e,k}$ as

$$H_{e,k} = \widehat{H}_{e,k} + \Delta H_{e,k}, g_{e,k} = \widehat{g}_{e,k} + \Delta g_{e,k}, \tag{10}$$

where $H_{e,k}$ and $g_{e,k}$ denote the true CSI; $\widehat{H}_{e,k}$ and $\widehat{g}_{e,k}$ denote the estimated CSI; $\Delta H_{e,k}$ and $\Delta g_{e,k}$ denote the associated CSI error, respectively. Specifically, the following bounded CSI models are considered, where the CSI error is assumed to lie in a region with a given bound, i.e.,

$$\mathcal{H}_{e,k} = \left\{ \left\| \Delta H_{e,k} \right\|_2 \leq \varepsilon_{e,k} \right\}, \mathcal{G}_{e,k} = \left\{ \left\| \Delta g_{e,k} \right\|_2 \leq \chi_{e,k} \right\}, \tag{11}$$

where $\varepsilon_{e,k}$ and $\chi_{e,k}$ denote the respective sizes of the bounded channel error region. As for the statistical error model, since it can be transformed into the bounded model by the proposed method in [20, 32], we focus on the bounded error model in this work due to the generality.

2.3. Problem Formulation. Our objective is to maximize the SEE by jointly designing w_k, v, and $\widehat{\boldsymbol{\theta}}$, subject to the maximum transmit power constraint and the unit modulus constraint (UMC). Here, we first relax the discrete phase shift design to the continuous phase shift design, then project the obtained solution to the discrete set. Mathematically, our problem is formulated as

$$\text{P1}: \max_{\mathrm{w_k}, \mathrm{v}, \widehat{\theta}} \quad \text{SEE}\left(\mathrm{w_k}, \mathrm{v}, \widehat{\boldsymbol{\theta}}\right) \tag{12(a)}$$

$$\text{s.t.} \sum_{k=1}^{K} \|w_k\|_2^2 + \|v\|_2^2 \leq P_{\max}, \tag{12(b)}$$

$$\left|\widehat{\theta}_m\right| = 1, \forall m \in M, \widehat{\theta}_{M+1} = 1. \tag{12(c)}$$

Notably, we find that P1 is nonconvex [34], which is hard to solve. In the next section, we will develop a tractable solution to P1 through convex approximation.

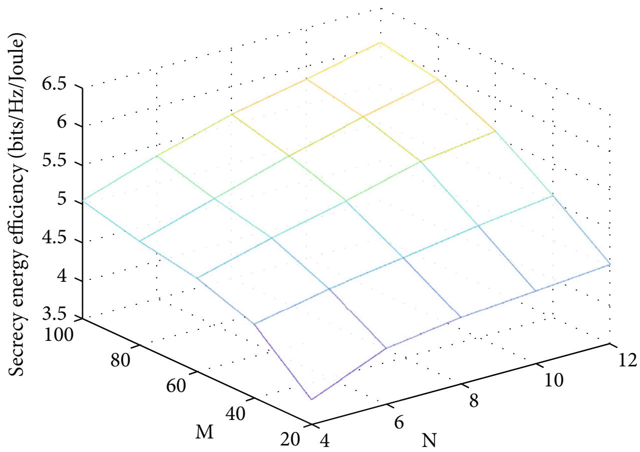

FIGURE 6: The SEE versus N and M.

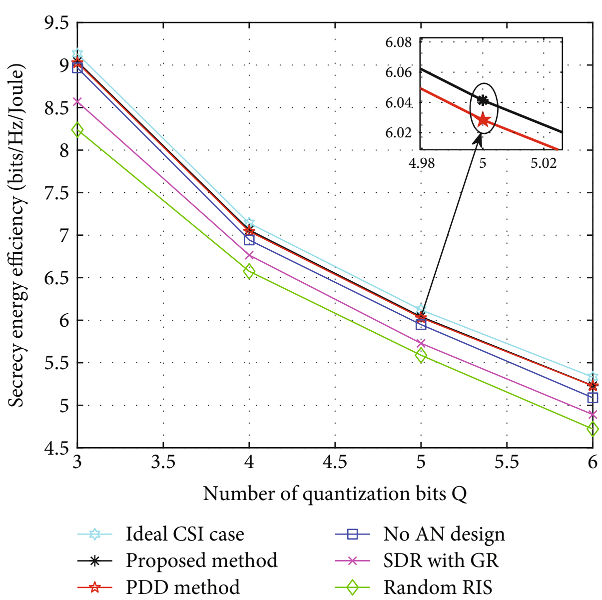

FIGURE 7: The SEE versus Q.

3. Proposed SEE Optimization Method

In this section, we will propose a SCA and CCCP based method to convert P1 into a solvable reformulation.

First, by introducing slack variables r_b and r_e, we recast P1 as

$$\mathrm{P2}: \max_{w_k, v, \widehat{\theta}, r_b, r_e} \frac{r_b - r_e}{\sum_{k=1}^{K} w_{k2}^{2} + v_{2}^{2} + P_c + MP_{\mathrm{RIS}}(Q)}, \tag{13(a)}$$

$$\text{s.t.} \frac{\left|\widehat{\theta}^H \bar{H}_k w_k\right|^2}{\sum_{i=1, i\neq k}^{K} \left|\widehat{\theta}^H \bar{H}_k w_i\right|^2 + \sigma_k^2} \geq 2^{r_b} - 1, \tag{13(b)}$$

$$\frac{\left|\widehat{\theta}^H \bar{H}_{e,k} w_k\right|^2}{\sum_{i=1, i\neq k}^{K} \left|\widehat{\theta}^H \bar{H}_{e,k} w_i\right|^2 + \left|\widehat{\theta}^H \bar{H}_{e,k} v\right|^2 + \sigma_{e,k}^2} \leq 2^{r_e} - 1. \tag{13(c)}$$

$$(12\mathrm{b}), (12\mathrm{c}). \tag{13(d)}$$

Then, via introducing auxiliary variables $p = [p_{1,1}, \cdots, p_{1,K}, p_{2,1}, \cdots, p_{2,K}, p_3]^T$ and $q = [q_{1,1}, \cdots, q_{1,K}, q_{2,1}, \cdots, q_{2,K}, q_3]^T$; P2 can be transformed into the following problem

$$\mathrm{P3}: \max_{w_k, v, \widehat{\theta}, r_b, r_e, p, q} \frac{r_b - r_e}{\sum_{k=1}^{K} \|w_k\|_2^2 + \|v\|_2^2 + P_c + MP_{\mathrm{RIS}}(b)} \tag{14(a)}$$

$$\text{s.t.} w_k^H \bar{H}_k^H \widehat{\theta}\widehat{\theta}^H \bar{H}_k w_k \geq p_{1,k}, \tag{14(b)}$$

$$\sum_{i=1, i\neq k}^{K} w_i^H \bar{H}_k^H \widehat{\theta}\widehat{\theta}^H \bar{H}_k w_i + \sigma_k^2 \leq \frac{1}{p_{2,k}}, \tag{14(c)}$$

$$p_{1,k} \geq p_3^2 / p_{2,k}, p_3^2 \geq 2^{r_b} - 1, \tag{14(d)}$$

$$w_k^H \bar{H}_{e,k}^H \widehat{\theta}\widehat{\theta}^H \bar{H}_{e,k} w_k \leq q_{1,k}^2, \tag{14(e)}$$

$$\sum_{i=1, i\neq k}^{K} w_i^H \bar{H}_{e,k}^H \widehat{\theta}\widehat{\theta}^H \bar{H}_{e,k} w_i + v^H \bar{H}_{e,k}^H \widehat{\theta}\widehat{\theta}^H \bar{H}_{e,k} v + \sigma_{e,k}^2 \geq q_{2,k}, \tag{14(f)}$$

$$q_{1,k}^2 / q_{2,k} \leq q_3, q_3 \leq 2^{r_e} - 1, \tag{14(g)}$$

$$(12\mathrm{b}), (12\mathrm{c}). \tag{14(h)}$$

Furthermore, to convert the fractional objective into a linear reformulation, we introduce auxiliary variables a_1, a_2, and a_3, P3 can be recast as the following problem

$$\mathrm{P4}: \max_{w_k, v, \widehat{\theta}, r_b, r_e, p, q, a_1, a_2, a_3 \geq 0} a_3 \tag{15(a)}$$

$$\text{s.t.} r_b - r_e \geq a_1, \tag{15(b)}$$

$$\sum_{k=1}^{K} \|w_k\|_2^2 + \|v\|_2^2 + P_c + MP_{\mathrm{RIS}}(b) \leq \frac{1}{a_2}, \tag{15(c)}$$

$$(14\mathrm{b}) - (14\mathrm{h}), \tag{15(d)}$$

$$a_3^2 \leq a_1 a_2. \tag{15(e)}$$

where we use the trick that maximize a_3^2 is equivalent to maximize a_3 to linear the objective.

P4 is still hard to solve due to the nonconvex constraints (15(c)) and (15(d)). In the following, we will utilize the SCA and CCCP to approximate these constraints. Firstly, we handle the first part of (14(d)) and (14(g)). In fact, $p_{1,k} \geq p_3^2/p_{2,k}$ is equivalent to $p_{1,k}p_{2,k} \geq p_3^2$. Moreover, $p_{1,k}p_{2,k} \geq p_3^2$ is equivalent to $(p_{1,k} + p_{2,k})^2 - (p_{1,k} - p_{2,k})^2 \geq 4p_3^2$, which can be

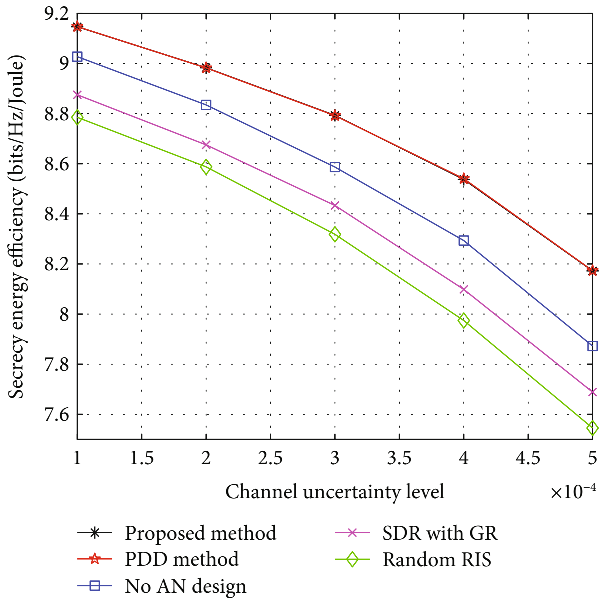

FIGURE 8: The SEE versus $\varepsilon_{e,k}^2$.

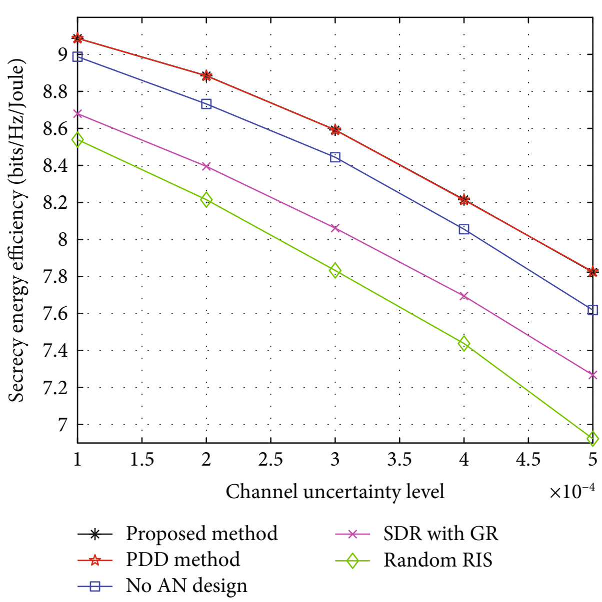

FIGURE 9: The SEE versus $\rho_{e,k}^2$.

further rewritten as

$$\left\| \left[2p_3, p_{1,k} - p_{2,k}\right] \right\|_2 \le p_{1,k} + p_{2,k}, \tag{16}$$

which is joint convex with respect to (w.r.t.) $\{p_{1,k}, p_{2,k}, p_3\}$. Similarly, $a_3^2 \le a_1 a_2$ and $q_{1,k}^2/q_{2,k} \le q_3$ can be equivalent rewritten as

$$\left\|[2a_3, a_1 - a_2]\right\|_2 \le a_1 + a_2, \left\| \left[2q_{1,k}, q_{2,k} - q_3\right] \right\|_2 \le q_{2,k} + q_3. \tag{17}$$

Then, we turn to the right hand side of (14(c)), (14(e)), (14(g)) and (15(c)) to handle the nonconvex functions $1/p_{2,k}$, $q_{1,k}^2$, 2^{r_e}, and $1/a_2$. In fact, in the $i+1$-th iteration, these constraints can be replaced by the following linear constraints

$$\sum_{i=1,i\neq k}^{K} w_i^H \bar{H}_k^H \widehat{\boldsymbol{\theta}}\widehat{\boldsymbol{\theta}}^H \bar{H}_k w_i + \sigma_k^2 \le \frac{2}{\bar{p}_{2,k}} - \frac{p_{2,k}}{\bar{p}_{2,k}^2}, \tag{18(a)}$$

$$w_k^H \bar{H}_{e,k}^H \widehat{\boldsymbol{\theta}}\widehat{\boldsymbol{\theta}}^H \bar{H}_{e,k} w_k \le 2q_{1,k}\bar{q}_{1,k} - \bar{q}_{1,k}^2, \tag{18(b)}$$

$$u_3 \le 2^{\bar{r}_e}\left((r_e - \bar{r}_e)\ln 2 + 1\right) - 1, \tag{18(c)}$$

$$\sum_{k=1}^{K} \|w_k\|_2^2 + \|v\|_2^2 + P_c + MP_{\mathrm{RIS}}(b) \le \frac{2}{\bar{a}_2} - \frac{a_2}{\bar{a}_2^2}, \tag{18(d)}$$

where $\bar{p}_{2,k}$, $\bar{q}_{1,k}$, $\bar{r}_e$, and $\bar{a}_2$ are the optimal values of $p_{2,k}$, $q_{1,k}$, r_e, and a_2 in the l-th iteration, respectively.

Then, we focus on the nonconvex (14(b) and 14(f)). In fact, these constraints can be turn to convex constraints w.r.t. a given variable when fixing the others. Actually, the left hand side of (14(b)) is convex w.r.t. w_k or $\widehat{\boldsymbol{\theta}}$ when fixing the others. Since a convex function can be lower-bounded or under-estimated by the first order Taylor expansion around a given point, thus, in the $i+1$-th iteration, (14(b)) can be approximated as

$$2\Re\left\{w_k^H \bar{H}_k^H \widehat{\boldsymbol{\theta}}\widehat{\boldsymbol{\theta}}^H \bar{H}_k \bar{w}_k\right\} - \bar{w}_k^H \bar{H}_k^H \widehat{\boldsymbol{\theta}}\widehat{\boldsymbol{\theta}}^H \bar{H}_k \bar{w}_k \ge p_{1,k}, \tag{19}$$

where $\bar{w}_k$ is the optimal values of w_k in the l-th iteration.

Then, (14(f)) can be approximated as

$$\begin{aligned}\sum_{i=1,i\neq k}^{K} &\left\{2\Re\left\{w_i^H \bar{H}_{e,k}^H \widehat{\boldsymbol{\theta}}\widehat{\boldsymbol{\theta}}^H \bar{H}_{e,k}\bar{w}_i\right\} - \bar{w}_i^H \bar{H}_{e,k}^H \widehat{\boldsymbol{\theta}}\widehat{\boldsymbol{\theta}}^H \bar{H}_{e,k}\bar{w}_i\right\} \\ &+ 2\Re\left\{v^H \bar{H}_{e,k}^H \widehat{\boldsymbol{\theta}}\widehat{\boldsymbol{\theta}}^H \bar{H}_{e,k}\bar{v}\right\} - \bar{v}^H \bar{H}_{e,k}^H \widehat{\boldsymbol{\theta}}\widehat{\boldsymbol{\theta}}^H \bar{H}_{e,k}\bar{v} \\ &+ \sigma_{e,k}^2 \ge q_{2,k},\end{aligned} \tag{20}$$

where $\bar{v}$ is the optimal values of v in the l-th iteration.

The remain task is to handle the CSI uncertainties in (18(b) and (20)). First, we denote $\tilde{H}_{e,k} = [\widehat{H}_{e,k}, \widehat{g}_{e,k}]^T$, and $\ddot{H}_{e,k} = [\Delta H_{e,k}, \Delta g_{e,k}]^T$; it is known that $\bar{H}_{e,k} = \tilde{H}_{e,k} + \ddot{H}_{e,k}$. Besides, the following equation holds

$$\left\|\Delta H_{e,k}\right\|_F \le \varepsilon_{e,k} \Rightarrow \left\|\mathrm{vec}(\Delta H_{e,k})\right\|_2 \le \varepsilon_{e,k}. \tag{21}$$

Then, we denote

$$I_1\Delta = \mathrm{Diag}\left(\underbrace{1\ldots1}_{MN}\ \underbrace{0\ldots0}_{N}\right), I_2\Delta = \mathrm{Diag}\left(\underbrace{0\ldots0}_{MN}\ \underbrace{1\ldots1}_{N}\right). \tag{22}$$

Thus, the following relationship holds

$$\ddot{h}_{e,k}^H I_1 \ddot{h}_{e,k} \le \varepsilon_{e,k}^2, \ddot{h}_{e,k}^H I_2 \ddot{h}_{e,k} \le \chi_{e,k}^2, \quad (23)$$

where $\ddot{h}_{e,k} = \mathrm{vec}(\ddot{H}_{e,k})$. We find the following extended S-Lemma is useful to handle the CSI uncertainty.

Lemma 2 (see [20]). *Define the function with variable $x \in \mathbb{C}^{n\times 1}$,*

$$f_j(x) = x^H A_j x + 2\,\mathrm{Re}\left\{b_j^H x\right\} + c_j, j = 0, \cdots, J, \quad (24)$$

where $A_j = A_j^H \in \mathbb{C}^{n\times n}$, $b_j \in \mathbb{C}^{n\times 1}$, and $c_j \in \mathbb{R}$. The condition $\{f_j(x) \ge 0\}_{j=1}^J \Rightarrow f_0(x) \ge 0$ holds if and only if there exists $\{\lambda_j \ge 0\}_{j=1}^J$ such that

$$\begin{bmatrix} \mathbf{A}_0 & \mathbf{b}_0 \\ \mathbf{b}_0^H & c_0 \end{bmatrix} - \sum_{j=1}^J \lambda_j \begin{bmatrix} \mathbf{A}_j & \mathbf{b}_j \\ \mathbf{b}_j^H & c_j \end{bmatrix} \succcurlyeq 0. \quad (25)$$

To utilize Lemma 2, we first denote $\bar{h}_{e,k} = \mathrm{vec}(\bar{H}_{e,k})$, $\tilde{h}_{e,k} = \mathrm{vec}(\tilde{H}_{e,k})$. By invoking the identity $\mathrm{Tr}(\boldsymbol{A}^H\mathbf{BCD}) = \mathrm{vec}(\mathbf{A})^H(\mathbf{D}^T \otimes \mathbf{B})\mathrm{vec}(\mathbf{C})$, (18(b)) can be rewritten as

$$\begin{aligned} &\tilde{h}_{e,k}^H\left(\left(w_k w_k^H\right)^T \otimes \widehat{\boldsymbol{\theta}}\widehat{\boldsymbol{\theta}}^H\right)\tilde{h}_{e,k} + \ddot{h}_{e,k}^H\left(\left(w_k w_k^H\right)^T \otimes \widehat{\boldsymbol{\theta}}\widehat{\boldsymbol{\theta}}^H\right)\ddot{h}_{e,k} \\ &+ 2\Re\left\{\tilde{h}_{e,k}^H\left(\left(w_k w_k^H\right)^T \otimes \widehat{\boldsymbol{\theta}}\widehat{\boldsymbol{\theta}}^H\right)\ddot{h}_{e,k}\right\} \le 2q_{1,k}\bar{q}_{1,k} - \bar{q}_{1,k}^2. \end{aligned} \quad (26)$$

Following Lemma 2, (26) holds if the following linear matrix inequality (LMI) holds

$$\begin{bmatrix} -\left(\mathbf{w}_k\mathbf{w}_k^H\right)^T \otimes \widehat{\boldsymbol{\theta}}\widehat{\boldsymbol{\theta}}^H + \alpha_{1,k}\mathbf{I}_1 + \alpha_{2,k}\mathbf{I}_2 & -\left(\left(\mathbf{w}_k\mathbf{w}_k^H\right)^T \otimes \widehat{\boldsymbol{\theta}}\widehat{\boldsymbol{\theta}}^H\right)\tilde{\mathbf{h}}_{e,k} \\ -\tilde{\mathbf{h}}_{e,k}^H\left(\left(\mathbf{w}_k\mathbf{w}_k^H\right)^T \otimes \widehat{\boldsymbol{\theta}}\widehat{\boldsymbol{\theta}}^H\right) & \rho_k \end{bmatrix} \succcurlyeq \mathbf{0}, \quad (27)$$

where $\{\alpha_{1,k} \ge 0, \alpha_{2,k} \ge 0\}_{k=1}^K$ are the slack variables, and $\rho_k = -\tilde{h}_{e,k}^H((w_k w_k^H)^T \otimes \widehat{\boldsymbol{\theta}}\widehat{\boldsymbol{\theta}}^H)\tilde{h}_{e,k} + 2q_{1,k}\bar{q}_{1,k} - \bar{q}_{1,k}^2 - \alpha_{1,k}\varepsilon_{e,k}^2 - \alpha_{2,k}\chi_{e,k}^2$.

Similarly, by denoting $\Phi_k = \sum_{i=1,i\ne k}^K w_i^H \bar{w}_i + \bar{w}_i^H w_i - \bar{w}_i^H \bar{w}_i + v^H\bar{v} + \bar{v}^H v - \bar{v}^H\bar{v}$, (20) is equivalent to

$$\begin{aligned} &\tilde{h}_{e,k}^H\left(\Phi_k^T \otimes \widehat{\boldsymbol{\theta}}\widehat{\boldsymbol{\theta}}^H\right)\tilde{h}_{e,k} + \ddot{h}_{e,k}^H\left(\Phi_k^T \otimes \widehat{\boldsymbol{\theta}}\widehat{\boldsymbol{\theta}}^H\right)\ddot{h}_{e,k} \\ &+ 2\Re\left\{\tilde{h}_{e,k}^H\left(\Phi_k^T \otimes \widehat{\boldsymbol{\theta}}\widehat{\boldsymbol{\theta}}^H\right)\ddot{h}_{e,k}\right\} + \sigma_{e,k}^2 \ge q_{2,k}. \end{aligned} \quad (28)$$

Then, by Lemma 2, we find that (28) holds if the following LMI holds

$$\begin{bmatrix} \boldsymbol{\Phi}_k^T \otimes \widetilde{\boldsymbol{\theta}}\widehat{\boldsymbol{\theta}}^H + \beta_{1,k}\mathbf{I}_1 + \beta_{2,k}\mathbf{I}_2 & \left(\boldsymbol{\Phi}_k^T \otimes \widehat{\boldsymbol{\theta}}\widehat{\boldsymbol{\theta}}^H\right)\tilde{\mathbf{h}}_{e,k} \\ \tilde{\mathbf{h}}_{e,k}^H\left(\boldsymbol{\Phi}_k^T \otimes \widehat{\boldsymbol{\theta}}\widehat{\boldsymbol{\theta}}^H\right) & \pi_k \end{bmatrix} \succcurlyeq \mathbf{0} \quad (29)$$

where $\{\beta_{1,k} \ge 0, \beta_{2,k} \ge 0\}_{k=1}^K$ are the slack variables, and $\pi_k = \tilde{h}_{e,k}^H(\Phi_k^T \otimes \widehat{\boldsymbol{\theta}}\widehat{\boldsymbol{\theta}}^H)\tilde{h}_{e,k} - \sigma_{e,k}^2 - \beta_{1,k}\varepsilon_{e,k}^2 - \beta_{2,k}\chi_{e,k}^2$.

Combining these steps, around given point $\{\bar{w}_k, \bar{v}, \overline{\boldsymbol{\theta}}, \bar{p}_{2,k}, \bar{p}_3, \bar{q}_{1,k}, \bar{q}_{2,k}, \bar{r}_e, \bar{a}_2\}$, we obtained the following approximated subproblem w.r.t. $\{w_k, v\}$

$$\mathrm{P5}: \max_{w_k, v, r_b, r_e, p, q, a_1, a_2} a_3 \quad (30a)$$

$$\begin{aligned} \mathrm{s.t.}\, p_3 \ge 2^{r_b} - 1, &(12b), (14e), (15b), (16), (17), \\ &(18a), (18c)(18d), (19), (25), (27), \end{aligned} \quad (30b)$$

which is convex and can be efficiently solved by the optimization toolbox, such as CVX [35].

Nextly, we handle these constraints w.r.t. $\widehat{\boldsymbol{\theta}}$ with fixed $\{w_k, v\}$. Here, we mainly focus on the difference between the counterpart of the optimization w.r.t. $\{w_k, v\}$. Firstly, (23) can be approximated as

$$2\Re\left\{\overline{\boldsymbol{\theta}}^H H_k w_k w_k^H H_k^H \widehat{\boldsymbol{\theta}}\right\} - \overline{\boldsymbol{\theta}}^H H_k w_k w_k^H H_k^H \overline{\boldsymbol{\theta}} \ge p_{1,k}, \quad (31)$$

where $\overline{\boldsymbol{\theta}}$ is the optimal values of $\widehat{\boldsymbol{\theta}}$ in the l-th iteration.

Then, for convenient, we denote $\Omega_k = vv^H + \sum_{i=1,i\ne k}^K w_i w_i^H$, thus, (14(c)) can be approximated as

$$\widehat{\boldsymbol{\theta}}^H H_k\left(\sum_{i=1,i\ne k}^K w_i w_i^H\right) H_k^H \widehat{\boldsymbol{\theta}} + \sigma_k^2 \le \frac{2}{\bar{p}_{2,k}} - \frac{p_{2,k}}{\bar{p}_{2,k}^2}, \quad (32)$$

and (14(f)) can be approximated as

$$2\Re\left\{\overline{\boldsymbol{\theta}}^H H_{e,k}\Omega_k H_{e,k}^H \widehat{\boldsymbol{\theta}}\right\} - \overline{\boldsymbol{\theta}}^H H_{e,k}\Omega_k H_{e,k}^H \overline{\boldsymbol{\theta}} + \sigma_{e,k}^2 \ge q_{2,k}. \quad (33)$$

Then, by Lemma 2, we find that (33) holds if the following LMI holds

$$\begin{bmatrix} \boldsymbol{\Omega}_k^T \otimes \widehat{\boldsymbol{\theta}}\overline{\boldsymbol{\theta}}^H + \beta_{1,k}\mathbf{I}_1 + \beta_{2,k}\mathbf{I}_2 & \left(\boldsymbol{\Omega}_k^T \otimes \widehat{\boldsymbol{\theta}}\overline{\boldsymbol{\theta}}^H\right)\tilde{\mathbf{h}}_{e,k} \\ \tilde{\mathbf{h}}_{e,k}^H\left(\boldsymbol{\Omega}_k^T \otimes \widehat{\boldsymbol{\theta}}\overline{\boldsymbol{\theta}}^H\right) & \pi_k \end{bmatrix} \succcurlyeq \mathbf{0}, \quad (34)$$

where $\{\beta_{1,k} \ge 0, \beta_{2,k} \ge 0\}_{k=1}^K$ are the slack variables, and $\pi_k = \tilde{h}_{e,k}^H(\Omega_k^T \otimes \widehat{\boldsymbol{\theta}}\overline{\boldsymbol{\theta}}^H)\tilde{h}_{e,k} - \sigma_{e,k}^2 - \beta_{1,k}\varepsilon_{e,k}^2 - \beta_{2,k}\chi_{e,k}^2$.

To this end, the only nonconvexity in P4 is the UMC (12(c)). In the following, we will utilize the penalty CCP method to handle (12(c)). According to the penalty CCP principle, (12(c)) can be first equivalently transformed into $1 \leq |\widehat{\theta}_m|^2 \leq 1$. Then, we introduce the following Lemma to handle the nonconvex part $1 \leq |\widehat{\theta}_m|^2$.

Lemma 3 (see [32]). *Let b be a complex scalar variable, then the following inequality holds*

$$\left|b^2\right| \geq \bar{b}^\dagger b + b^\dagger \bar{b} - \bar{b}^\dagger \bar{b}, \tag{35}$$

for any fixed point ã.

Via Lemma 3, the subproblem w.r.t. $\widehat{\boldsymbol{\theta}}$ can be formulated as

$$\text{P6}: \max_{\widehat{\theta},r_b,r_e,p,q,a_1,a_2,a_3,b} \quad a_3 - \lambda^{[l]} \sum_{m=1}^{M} b_m, \tag{36(a)}$$

$$\text{s.t.} \left|\widehat{\theta}_m\right|^2 \leq 1 + b_m, \forall m, \tag{36(b)}$$

$$-\bar{\theta}_m^* \widehat{\theta}_m - \widehat{\theta}_m^* \bar{\theta}_m + \bar{\theta}_m^* \bar{\theta}_m \leq b_m - 1, \forall m, \tag{36(c)}$$

$$p_3 \geq 2^{r_b} - 1, (12b), (14e), (15b), (16), (17), (18c), (18d), (29), (30), (32), \tag{36d}$$

where $\bar{\theta}_m$ is the obtained $\widehat{\theta}_m$ in the previous iteration; $b = [b_1, \cdots, b_M]^T \in \mathbb{C}^{M\times 1}$ is the slack variable for the UMC, and $\lambda \geq 0$ is the penalty multiplier to scale the penalty item $\sum_{m=1}^{M} b_m$, which can control the feasibility of $\widehat{\boldsymbol{\theta}}$. Here, $\lambda^{[l]}$ is updated by $\lambda^{[l]} = \min\{\gamma\lambda^{[l-1]}, \lambda_{\max}\}$, where the upper bound $\lambda_{\max}$ is used to avoid numerical problems. More details can refer to [27, 32].

To this end, we have solved P1 efficiently. The whole procedure is summarized in Algorithm 3, where WSR^l is the obtained optimal value in the l-th iteration for P1. In addition, ς denotes the accuracy.

Thus, we have finished the algorithm in the continuous phase shift case. While for the discrete phase shift case, at the end of Algorithm 1, we project the obtained θ_m into the discrete set. In particular, we denote the solution of the two cases as θ_m^{c} and θ_m^{d}, respectively. Then, we map θ_m^{c} to obtain θ_m^{d}, i.e., $\theta_m^{\mathrm{d}} = e^{j\phi_{u^{å}}}$, where $u^{å} = \operatorname*{argmin}_{1\leq u\leq \tau} |\theta_m^{\mathrm{c}} - e^{j\phi_q}|$.

4. Simulation Results

In this section, we provide simulation results to assess the performance of the proposed algorithm. The simulation scenario is shown in Figure 2, where there are one Alice, one RIS, 4 Bobs, and 4 Eves. A three dimensional coordinate system is utilized to represent the positions of these nodes, where Alice and RIS are deployed at (0 m, 0 m, and 10 m) and (50 m, 10 m, and 10 m), while all Bobs/Eves are randomly located in a circle centered at (50 m, 0 m, and 2 m) and with radius 5 m. In fact, the electromagnetic feature of each reflecting element can be adapted. Thus, by proper designing the phase of each reflecting element, the incident signal can be reflected to different direction to serve different users. Besides, the distance between these users is commonly smaller than the distance between the Alice to RIS, and the RIS is deployed more closer to the users than the Alice. Thus, the RIS does not need to form a very thin reflecting beam.

Unless otherwise specified, the simulation settings are assumed as follows: $N = 4$, $M = 40$, $Q = 3$, $P_{\max} = -20$dBW, $P_c = -40$dBm, and $\sigma_k^2 = \sigma_{e,k}^2 = -80$dBm, $\forall k$. The large-scale path loss is given by $\mathrm{PL} = \mathrm{PL}_0 - 10\alpha \log_{10}(d/d_0)$, where PL_0 is the path loss at the reference distance d_0; d is the link distance; α is the path loss exponent. More details about the simulation parameters can refer to [36]. As for the CSI uncertainty, we use a parameter to model the uncertainty, which is given as $\varepsilon_{e,k}^2 = \varepsilon_{e,k}^2 \|\widehat{H}_{e,k}\|_F^2$, and $\chi_{e,k}^2 = \rho_{e,k}^2 \|\widehat{g}_{e,k}\|_2^2$, respectively, where $\varepsilon_{e,k}$ and $\rho_{e,k}$ measure the relative number of the CSI errors and are set as $\varepsilon_{e,k}^2 = 10^{-4}$ and $\rho_{e,k}^2 = 10^{-4}$ [32], respectively. In addition, for the parameters of the CCCP method, we set $\lambda^{[1]} = 20$, $\lambda_{\max} = 10$, and $\gamma = 0.8$ [27].

Here, we compare the proposed method with the following benchmarks: (1) the no AN design, e.g., setting $z = 0$ while only optimizing w_k and $\widehat{\boldsymbol{\theta}}$; (2) the random RIS design, e.g., choosing $\widehat{\boldsymbol{\theta}}$ randomly; (3) the no RIS-assisted case; (4) Alice can obtain ideal CSI of the Eves, which can be seen as the upper bound of the proposed design; (5) the penalty dual decomposition (PDD) method in [20]; (6) the SDR with Gaussian randomization (GR) methods [4]. These designs are labeled as "Proposed method", "No AN design", "Random RIS", "No RIS case", "Ideal CSI case", "PDD method", and "SDR with GR", respectively.

Firstly, we investigate the convergence behaviour of the proposed method by comparing the obtained SEE with the number of iterations. Figure 3 shows the convergence behaviour with different number of N and M via fixing all the other parameters. From this figure, we can see that the proposed method can always converge to the optimal solution in almost 20 iterations, which suggests the convergence of the proposed method. Besides, it should be pointed that in the simulation, we utilize the obtained objective value of P5, e.g., a_3 in (50) to judge the secrecy energy efficiency. This is mainly due to the fact that there exists a penalty term $-\lambda^{[l]}\sum_{m=1}^{M} b_m$ in the objective of P6, thus using the obtained objective value of P5 to judge the secrecy energy efficiency is more straightforward.

Then, we compare the SEE of these schemes versus the transmit power budget $P_{\max}$, the result is shown in Figure 4. From this figure, we can see that the proposed method achieves the very closed performance with the PDD method, and outperforms the SDR with GR method. In addition, for all these methods, the SEE tends to increase with $P_{\max}$ only when $P_{\max}$ is smaller than a threshold and then the SEE approaches a constant when $P_{\max}$ is larger than the threshold value. This is due to the fact that there exists a unique maximizer of the transmit power for SEE maximization and the SEE saturates when the power budget exceeds the value of this maximizer. Consequently, the actual transmit power remains constant when the maximum SEE is attained, leading to saturated SEE in high $P_{\max}$ regimes. To provide more insights for this results, the corresponding secrecy rate is reported versus $P_{\max}$ in Figure 5, where we can see that the secrecy rate increases rapidly with $P_{\max}$ when $P_{\max}$ is small and then increases slowly when $P_{\max}$ is large. Thus, using all the available power budget to maximize the secrecy rate is not a sound strategy from the perspective of the energy efficiency. Besides, it is also observed that the no AN method achieves nearly performance with the proposed method, while the no RIS and random RIS methods suffer certain performance loss, especially for the no RIS design, which suggests that RIS play a more important role than AN in improving the performance.

Next, we show the obtained SEE of the proposed method versus N and M; the result is shown in Figure 6. From this figure, we can see that the SEE increases monotonically with N and M. This is due to that larger N or M leads to higher secrecy rate, thus to improve the SEE. In addition, we can see that M plays a more important role on the SEE performance than N, since the RIS utilizes passive elements, no radio frequency chains will be required, thus lower power consumption can be obtained.

Moreover, we compare the SEE of these schemes versus the number of quantization bits Q; the result is shown in Figure 7. From this figure, we can see that for all these RIS-aided methods, the SEE decreases monotonically with Q. This is mainly due to the fact that the increase of Q can only increase the secrecy rate slightly but lead a significant increase of the quantization energy consumption, thus decrease the SEE.

Finally, we show the SEE of these schemes versus the CSI uncertainty level $\varepsilon_{e,k}^2$ and $\rho_{e,k}^2$ in Figures 8 and 9, respectively. From these two figures, we find that the SEE decreases when the uncertainty level increases. This phenomenon indicated that the CSI uncertainty level has nonnegligible impact on the secure performance. Since the larger CSI uncertainty level, the higher probability that the confidential information leakage to the Eve's channel. In addition, by comparing Figure 8 with Figure 9, we can see that the CSI uncertainty of the cascaded channel plays a more dominating role than that of the direct channels in the SEE performance.

5. Conclusion

In this paper, we have investigated the robust SEE optimization in a RIS-assisted wiretap channels. Specifically, we aim to maximize the worst case SEE via jointly designing the BF, the AN covariance, and the phase shifter. Different with the commonly used Dinkelbach algorithm, we transformed the fractional programming into a solvable problem with linear objective, while all the constraints are approximated via SCA and CCCP. Then, an iterative method was proposed to solve the approximated convex problem. Simulation results demonstrated the performance of the proposed design.

Data Availability

Data available on request.

Conflicts of Interest

The authors declare that there are no conflicts of interest regarding the publication of this article.

Acknowledgments

This work was supported in part by the Natural Science Foundation of China under Grant No. 61673108, in part by the Colleges and Universities Natural Science Foundation in Jiangsu Province under Grant No.19KJA110002, and in part by the Industry-University-Research Cooperation Project of Jiangsu Province No. BY2020335 and No. BY2020358.

References

[1] M. Zhao, Q. Shi, and M. Zhao, "Efficiency maximization for UAV-enabled mobile relaying systems with laser charging," *IEEE Transactions on Wireless Communications*, vol. 19, no. 5, pp. 3257–3272, 2020.

[2] Q. Wu, S. Zhang, B. Zheng, C. You, and R. Zhang, "Intelligent reflecting surface-aided wireless communications: a tutorial," *IEEE Transactions on Communications*, vol. 69, no. 5, pp. 3313–3351, 2021.

[3] C. Huang, A. Zappone, G. C. Alexandropoulos, M. Debbah, and C. Yuen, "Reconfigurable intelligent surfaces for energy efficiency in wireless communication," *IEEE Transactions on Wireless Communications*, vol. 18, no. 8, pp. 4157–4170, 2019.

[4] F. Fang, Y. Xu, Q.-V. Pham, and Z. Ding, "Energy-efficient design of IRS-NOMA networks," *IEEE Transactions on Vehicular Technology*, vol. 69, no. 11, pp. 14088–14092, 2020.

[5] M. Zeng, E. B. Mohamed, O. A. Dobre, P. Fortier, and Q.-V. Pham, "Energy-efficient resource allocation for IRS-assisted multi-antenna uplink systems," *IEEE Wireless Communications Letters*, vol. 10, no. 6, pp. 1261–1265, 2021.

[6] Q. N. Le, V. D. Nguyen, and O. A. Dobre, "Energy efficiency maximization in RIS-aided cell-free network with limited backhaul," *IEEE Communications Letters*, vol. 25, no. 6, pp. 1974–1978, 2021.

[7] Y. Zhang, B. Di, H. Zhang, J. Lin, Y. Li, and L. Song, "Beyond cell-free MIMO: energy efficient reconfigurable intelligent surface aided cell-free MIMO communications," *IEEE Transactions on Cognitive Communications and Networking*, vol. 7, no. 2, pp. 412–426, 2021.

[8] Z. Yang, M. Chen, W. Saad et al., "Energy-efficient wireless communications with distributed reconfigurable intelligent surfaces," *IEEE Transactions on Wireless Communications*, vol. 21, no. 1, pp. 665–679, 2022.

[9] S. Jia, X. Yuan, and Y.-C. Liang, "Reconfigurable intelligent surfaces for energy efficiency in D2D communication network," *IEEE Wireless Communications Letters*, vol. 10, no. 3, pp. 683–687, 2021.

[10] S. Zargari, A. Khalili, Q. Wu, M. R. Mili, and D. W. K. Ng, "Max-min fair energy-efficient beamforming design for intelligent reflecting surface-aided SWIPT systems with non-linear

energy harvesting model," *IEEE Transactions on Vehicular Technology*, vol. 70, no. 6, pp. 5848–5864, 2021.

[11] L. You, J. Xiong, D. W. K. Ng, C. Yuen, W. Wang, and X. Gao, "Energy efficiency and spectral efficiency tradeoff in RIS-aided multiuser MIMO uplink transmission," *IEEE Transactions on Signal Processing*, vol. 69, pp. 1407–1421, 2021.

[12] D. Wang, F. Zhou, W. Lin, Z. Ding, and N. Al-Dhahir, "Cooperative hybrid nonorthogonal multiple access-based mobile-edge computing in cognitive radio networks," *IEEE Transactions on Cognitive Communications and Networking*, vol. 8, no. 2, pp. 1104–1117, 2022.

[13] D. Wang, Y. He, K. Yu, G. Srivastava, L. Nie, and R. Zhang, "Delay-sensitive secure NOMA transmission for hierarchical HAP-LAP medical-care IoT networks," *IEEE Transactions on Industrial Informatics*, vol. 18, no. 8, pp. 5561–5572, 2022.

[14] D. Wang, T. He, F. Zhou, J. Cheng, R. Zhang, and Q. Wu, "Outage-driven link selection for secure buffer-aided networks," *SCIENCE CHINA Information Sciences*, vol. 65, no. 8, pp. 1–6, 2022.

[15] Y. He, L. Nie, T. Guo, K. Kaur, M. M. Hassan, and K. Yu, "A NOMA-enabled framework for relay deployment and network optimization in double-layer airborne access VANETs," *IEEE Transactions on Intelligent Transportation Systems*, vol. 1, pp. 1–15, 2022.

[16] L. Dong and H. Wang, "Enhancing secure MIMO transmission via intelligent reflecting surface," *IEEE Transactions on Wireless Communications*, vol. 19, no. 11, pp. 7543–7556, 2020.

[17] Z. Chu, W. Hao, P. Xiao et al., "Secrecy rate optimization for intelligent reflecting surface assisted MIMO system," *IEEE transactions on information forensics and security*, vol. 16, pp. 1655–1669, 2021.

[18] Y. Liu, X. Liu, X. Mu et al., "Reconfigurable intelligent surfaces: principles and opportunities," *IEEE Communications Surveys & Tutorials*, vol. 23, no. 3, pp. 1546–1577, 2021.

[19] C. Pan, G. Zhou, K. Zhi et al., "An overview of signal processing techniques for RIS/IRS-aided wireless systems," *IEEE Journal of Selected Topics in Signal Processing*, vol. 16, no. 5, pp. 883–917, 2022.

[20] H. Niu, Z. Chu, F. Zhou, Z. Zhu, L. Zhen, and K.-K. Wong, "Robust design for intelligent reflecting surface-assisted secrecy SWIPT network," *IEEE Transactions on Wireless Communications*, vol. 21, no. 6, pp. 4133–4149, 2022.

[21] X. Wu, J. Ma, C. Gu, X. Xue, and X. Zeng, "Secure and energy efficient transmission for IRS-assisted cognitive radio networks," *IEEE Transactions on Cognitive Communications and Networking*, vol. 8, no. 1, pp. 170–185, 2022.

[22] Q. Wang, F. Zhou, R. Q. Hu, and Y. Qian, "Energy efficient robust beamforming and cooperative jamming design for IRS-assisted MISO networks," *IEEE Transactions on Wireless Communications*, vol. 20, no. 4, pp. 2592–2607, 2021.

[23] J. Liu, K. Xiong, Y. Lu, D. W. K. Ng, Z. Zhong, and Z. Han, "Energy efficiency in secure IRS-aided SWIPT," *IEEE Wireless Communications Letters*, vol. 9, no. 11, pp. 1884–1888, 2020.

[24] S. Zhang and R. Zhang, "Capacity characterization for intelligent reflecting surface aided MIMO communication," *IEEE Journal on Selected Areas in Communications*, vol. 38, no. 8, pp. 1823–1838, 2020.

[25] Z. Zhou, N. Ge, Z. Wang, and L. Hanzo, "Joint transmit precoding and reconfigurable intelligent surface phase adjustment: a decomposition-aided channel estimation approach," *IEEE Transactions on Communications*, vol. 69, no. 2, pp. 1228–1243, 2021.

[26] Z. Wang, L. Liu, and S. Cui, "Channel estimation for intelligent reflecting surface assisted multiuser communications: framework, algorithms, and analysis," *IEEE Transactions on Wireless Communications*, vol. 19, no. 10, pp. 6607–6620, 2020.

[27] G. Zhou, C. Pan, H. Ren, K. Wang, M. D. Renzo, and A. Nallanathan, "Robust beamforming design for intelligent reflecting surface aided MISO communication systems," *IEEE Wireless Communications Letters*, vol. 9, no. 10, pp. 1658–1662, 2020.

[28] X. Yu, D. Xu, Y. Sun, D. W. K. Ng, and R. Schober, "Robust and secure wireless communications via intelligent reflecting surfaces," *IEEE Journal on Selected Areas in Communications*, vol. 38, no. 11, pp. 2637–2652, 2020.

[29] M. M. Zhao, A. Liu, and R. Zhang, "Outage-constrained robust beamforming for intelligent reflecting surface aided wireless communication," *IEEE Transactions on Signal Processing*, vol. 69, pp. 1301–1316, 2021.

[30] S. Hong, C. Pan, H. Ren, K. Wang, K. K. Chai, and A. Nallanathan, "Robust transmission design for intelligent reflecting surface-aided secure communication systems with imperfect cascaded CSI," *IEEE Transactions on Wireless Communications*, vol. 20, no. 4, pp. 2487–2501, 2021.

[31] K. Ntougias and I. Krikidis, "Robust design of secure IRS-aided MISO broadcasting for SWIPT and spectrum sharing," in *2021 IEEE Global Communications Conference (GLOBECOM)*, pp. 1–7, Madrid, Spain, 2021.

[32] G. Zhou, C. Pan, H. Ren, K. Wang, and A. Nallanathan, "A framework of robust transmission design for IRS-aided MISO communications with imperfect cascaded channels," *IEEE Transactions on Signal Processing*, vol. 68, pp. 5092–5106, 2020.

[33] M. M. Zhao, Q. Wu, M. J. Zhao, and R. Zhang, "Exploiting amplitude control in intelligent reflecting surface aided wireless communication with imperfect CSI," *IEEE Transactions on Communications*, vol. 69, no. 6, pp. 4216–4231, 2021.

[34] S. Boyd and L. Vandenberghe, *Convex Optimization*, Cambridge University Press, Cambridge, U.K., 2004.

[35] M. Grant and S. Boyd, "CVX: Matlab software for disciplined convex programming [online]," Avaiable: http://cvxr.com/cvx/.

[36] H. Niu, Z. Chu, F. Zhou, Z. Zhu, M. Zhang, and K.-K. Wong, "Weighted sum secrecy rate maximization using intelligent reflecting surface," *IEEE Transactions on Communications*, vol. 69, no. 9, pp. 6170–6184, 2021.